Targeting Degradation of RNA by RNase H Using DNA Hairpins†

Jing Li,‡ Brooke Bourdelat-Parks,‡ Jeffrey H. Boatright,§ and Roger M. Wartell*,‡

School of Biology, Georgia Institute of Technology, Atlanta, Georgia 30332-0230, and Department of Ophthalmology, Emory Eye Center, Emory University School of Medicine, Atlanta, Georgia 30322

Received May 27, 2003; Revised Manuscript Received July 17, 2003

ABSTRACT: RNase H degradation of two 15 nt RNA target sites was examined in the presence of hairpin DNAs with a 5 nt loop and a 10 bp stem or single-stranded 15 nt DNAs. One target site was a segment of a 79 nt RNA, and the other was part of a 53 nt RNA. Secondary structure predictions indicate that the 53 nt RNA target site is entirely single stranded, while a portion of the 79 nt RNA target site forms an intramolecular duplex. Less RNase H and DNA were needed to cleave the 53 nt RNA target site than the less accessible 79 nt RNA site. The hairpin DNAs had their 5 nt loop and 3′ side of the stem fully complementary to the target sites or had sequence changes that produced one to nine mismatched pairs. T_m values ranged from 57 to 80 °C. The stability of the hairpin DNAs relative to the stability of their corresponding RNA−DNA hybrids influenced the extent of RNase H degradation at 37 °C. Under the assay conditions employed, the amount of degradation directed by the hairpin DNAs was correlated with their predicted $\Delta G°_{37}$ of binding to the RNA targets. A DNA hairpin with one mismatch to the target site of the 79 nt RNA did not induce degradation under conditions where fully complementary DNA hairpins produced 50−80% degradation. The in vitro results indicate that DNA hairpins can enhance the stringency of RNase H targeted degradation of the RNA sites.

Antisense technology aims to inhibit expression of a specific gene by using short oligodeoxynucleotides (ODNs) that bind by Watson−Crick base pairing to a complementary sequence in a target RNA. The DNA/RNA hybrid may alter the processing or translation of a transcribed RNA and prevent expression of the encoded protein. Evidence indicates that the ubiquitous enzyme RNase H can play an important role in antisense inhibition of gene expression presumably by degrading the RNA strand of the RNA/DNA hybrid formed by the antisense ODN[1] (*1*−*3*).

Antisense ODNs have been used to help determine or validate a gene's function in vivo (*4*). They have also been investigated as possible therapeutic agents for many human diseases. In principle, effective antisense ODNs can mitigate diseases that are caused by the expression of an abnormal gene product or the overexpression of a normal gene. Antisense ODNs are being tested for the treatment of viral infections (*5*, *6*), cancer (*7*−*11*), and other diseases (*12*, *13*).

Among the technical problems encountered in applying antisense ODNs in vivo are their intracellular degradation by nucleases and insufficient target specificity. Modifications to the backbone of ODNs have been developed that increase their stability against nuclease degradation. Phosphorothioate ODNs were found to be resistant to nuclease hydrolysis in biological fluids (*14*) and can direct RNase H to cleave the hybridized RNA. Morpholino ODNs have also been shown to be resistant to degradative enzymes (*15*) and to be effective as antisense agents in cell translation systems (*16*). Other modifications of the backbone have been explored with varying success in their ability to bind a target site and support antisense activity (*1*, *17*).

The problem of insufficient target specificity encountered with phosphodiester and phosphorothioate ODNs appears to be due to the partial base pairing of an ODN to nontargeted RNA sequences that still permit RNase H degradation (*18*). A recent strategy used to reduce nonspecific RNase H cleavage is to utilize mixed-backbone ODNs (*19*−*24*) with one or two segments that do not support RNase H activity due to modifications such as methylphosphonate and 2′-methoxyribose linkages. A different antisense approach employs ODNs with a phosphoroamidate linked morpholino backbone. These oligomers do not support RNase H activity but exhibit high binding affinity to complementary RNA sequences and can directly block translation (*17*). Although target specificity is improved, nonspecific antisense effects due to hybridization to nontargeted RNAs may also occur in these approaches.

Previous studies have shown that a hairpin DNA can direct the degradation of a complementary RNA sequence by RNase H (*25*). DNA hairpins may also offer an advantage because their structure is less susceptible to nuclease degradation than a single-stranded molecule (*26*). Antisense hairpin DNAs have been shown to have high stability in fetal calf serum and human plasma (*27*). In this study, we explored the ability of DNA hairpins and single-stranded ODNs to direct RNase H digestion at 15 nt long target sites within 79 and 53 nt RNA molecules. The hairpin DNAs were comprised of a 10 bp stem and 5 nt loop and had a 15 nt segment that was either fully or partially complementary to the RNA target sites.

† This work was supported by the Emory Georgia Tech Biomedical Research Center.

* To whom correspondence should be addressed. E-mail: roger.wartell@biology.gatech.edu.

‡ Georgia Institute of Technology.

§ Emory University School of Medicine.

[1] Abbreviations: nt, nucleotide; bp, base pairs; RNase H, ribonuclease H; ODNs, oligodeoxyribonucleotides.

10.1021/bi034897z CCC: $25.00
Published on Web 08/26/2003

Thermodynamic calculations were used to estimate the free energy of formation of RNA/DNA duplexes formed by the DNA hairpins and their RNA targets. The correlation between the free energies of formation and the ability of the hairpin DNAs to direct degradation of the RNA in an RNase H assay was examined. The objective was to determine if thermodynamic considerations can guide the selection of a hairpin DNA that directs RNase H cleavage at a fully complementary RNA site but does not direct degradation of RNA sequences with one or a few mismatches. Results indicate that under appropriate conditions, RNaseH degradation of RNA sites directed by hairpin DNAs is correlated with the free energy of DNA/RNA binding and can enhance the stringency of RNA site cleavage.

MATERIALS AND METHODS

Preparation of the Oligonucleotides. Oligonucleotides were obtained from Qiagen Operon Technologies, Inc., Alameda, CA, or from the Emory University Microchemical Facility, Atlanta, GA. The ODNs were purified by reverse-phase HPLC and characterized by PAGE. Concentrations were determined from UV absorbance measurements of ODN solutions at 260 nm and the Oligosol program (*28*). For hairpin DNAs, absorbance was determined at temperatures (85−95 °C) where the DNAs were single stranded and linearly extrapolated back to 25 °C.

Plasmid Construction. The two plasmids employed for in vitro transcription of the RNA target molecules were constructed by inserting either a sequence from the HIV-1 genome or a sequence from the 5′ end of the chloramphenicol acetyltransferase (CAT) gene into the multiple cloning site of the pGEM7Zf+ plasmid (Promega Corp.). The plasmid designated pN1 was described earlier (*25*). It has a 30 nt sequence from the HIV-1 MN strain containing 10 consecutive pyrimidines inserted between the *Apa* I and the *EcoR* I restriction sites of the pGEM7Zf(+) plasmid. The second plasmid, pCAT16, was constructed by inserting a 16 nt sequence from the chloramphenicol acetyltransferase (CAT) gene translation initiation site between the *Apa* I and the *EcoR* I restriction sites of the pGEM7Zf(+) plasmid. Two partially complementary oligomers (5′-GCGC**GGGCCC**-TAAGATGGAGAAAAAAA-3′, and 5′-GTCG**GAATTC**-TGATTTTTTTCTCCATC-3′) were hybridized and filled in by Taq DNA polymerase. The CAT sequence is underlined, and the *Apa* I and *EcoR* I sites are shown in bold. A *Dde* I site (5′-CTAAG-3′) occurs in this sequence.

The DNA oligomer duplex and pGEM7Zf(+) plasmid were digested with *Apa*I and *Eco*RI. The linearized pGem7Zf+ plasmid was treated with calf intestinal alkaline phosphatase (Promega Inc.), and the restriction enzyme-cut DNA oligomers were ligated downstream of the T7 promoter sequence in pGEM7Zf(+) using T4 ligase. The modified plasmid was then transformed into *Escherichia coli* JM109 cells (Promega, Inc.). Modified plasmids were initially identified by digesting with *Dde*I, which produces five fragments instead of the four fragments produced from pGEM7Zf(+). DNA sequencing verified the correct insert.

In Vitro Transcription Reaction and RNA Purification. RNA transcripts 79 and 53 nt long were produced using the *Hind* III digested pN1 plasmid or the *Csp45* I digested pCAT16 plasmid as templates for T7 RNA polymerase. The 1 mL transcription reactions contained 10 mM dithiothreitol (100 μL of 100 mM DTT); 500 μM each of ATP, CTP, GTP, and UTP (200 μL of a mix with 2.5 mM of each NTP); 1X transcription buffer or 50 mM Tris-HCl, pH 7.5, 10 mM $NaCl_2$, 6 mM $MgCl_2$, and 2 mM spermidine; 50 μL of Prime RNA inhibitor (0.5 unit/μL) (Eppendorf Inc., Boulder, CO); 100 μL of 1 mg/mL BSA; 60 μL of 2 units/μL T7 RNA polymerase; 100 μg of the digested plasmid DNA; and 180 μL of RNase-free H_2O. Transcription reactions were carried out in a 37 °C water bath for 3 h. After the reaction, the plasmid template was separated from the remaining reaction components with a Centricon-100 concentrator (Millipore Co., Bedford, MA). The filtrate was collected and transferred to a Centricon-10 concentrator and centrifuged at 1000*g* to concentrate the RNA and to remove smaller molecules from the reaction mixture. The last step was repeated two more times. The RNA concentration was estimated by assuming 1.0 OD of RNA measured at 260 nm at 25 °C corresponds to approximately 40 μg/mL (*29*).

Melting Curve Characterization of Oligodeoxyribonucleotides. UV absorbance melting transitions were employed to characterize the oligodeoxynucleotides. A DMS 300 or Cary 1E spectrophotometer (Varian Inc., Palo Alto, CA) was used to obtain melting curves at 268 nm. Samples were heated at a rate of 0.5 °C/min in the 1X RNase H buffer (20 mM KCl, 10 mM $MgCl_2$, 20 mM Tris-HCl (pH 7.5), 0.1 mM Na_2EDTA). Absorbance and temperature measurements were collected from 15 to 90 °C using DNA concentrations of 1.5 uM. Eight-fold higher concentrations were used for several samples. T_m values were determined from the normalized melting curves as described previously (*25*). Average values listed are reproducible within ±1.0 °C.

Thermodynamic Analysis of ODN−RNA Interactions. The amount of hybrid formed between a DNA oligomer and its RNA target site was estimated based on the free energies of the RNA/DNA, RNA, and DNA secondary structures. The nearest neighbor model of nucleic acid stability was employed (*30*, *31*) using the empirically determined free energies of nucleic acid structural elements (*32*−*35*). Free energies of structural elements that have not yet been determined were estimated as described next.

The free energy of formation of a RNA/DNA duplex from its constituent single strands was calculated using the free energies for helix initiation and base pair stacking (35) as well as dangling ends or mismatched base pairs when appropriate. Free energy values are not yet available for terminal mismatches or dangling bases at the ends of an RNA/DNA duplex. Table 1 shows the free energy contribution of some terminal mismatches and single base dangling ends evaluated for RNA and DNA duplexes (*30*, *36*). Since many of the sequence-related ends (e.g., dCC/dG and rCC/rG) contributed similar ΔG values to RNA and DNA duplexes, we assumed that the ΔG contribution of a terminal mismatch or dangling end to an RNA/DNA duplex was the same as the analogous element ending an RNA duplex (*30*). For example, the 5′ dangling end rCC/dG and terminal mismatch rAA/dAT expected to occur in hybrids produced by DNA hairpin oligomers and the 79 nt RNA were assigned ΔG values of −0.3 and −0.8 kcal/mol, respectively (Table 1). Recently, Ohmichi et al. (*37*) showed that dangling ends of two to four adenines enhance the stability of RNA and DNA duplexes beyond that of a single dangling adenine by 0.1−1.0 kcal/mol. We assumed that extended RNA and DNA

Table 1: List of Free Energy Values (kcal/mol) for Terminal Mismatches and Dangling Ends Used in the Calculation of RNA/DNA Formation and the Corresponding Values for RNA (*30*) and DNA Duplexes (*36*)[a]

terminal mismatches/ dangling ends	ΔG in RNA duplex	ΔG in DNA duplex	ΔG value used for RNA/DNA duplex	occurred in the following ODNs:
5′ CC 3′ 3′ G 5′	−0.3	−0.52	−0.3	H0A, H0B, H1A, H2A, H4A, S15-0A, S15-1A, S15-2A, S15-3A, S15-4A
5′ AA 3′ 3′ TA 5′	−0.8	−0.63	−0.8	H0A, H0B, H1A, H2A, H2b, h4b, H5A
5′ AA 3′ 3′ T 5′	−0.8	−0.12	−0.8	S15-0A, S15-1A, S15-2A, S15-3A, S15-4A, S15-4B
5′ GA 3′ 3′ CC 5′	−1.5	−1.4	−1.5	S19
5′ AG 3′ 3′ TA 5′	−0.8	−0.51	−0.8	H4A
5′ GC 3′ 3′ CC 5′	−0.7	−0.75	−0.7	H2B, H3A, H4B, S15−3A
5′ AU 3′ 3′ TT 5′	−0.8	0.03	−0.8	H3A, H5A, S15-5A
5′ AA 3′ 3′ T 5′	−0.8	−0.51	−0.8	S15-5A
5′ UA 3′ 3′ T 5′	−0.3	−0.71	−0.3	Hcat0A
5′ CA 3′ 3′ GA 5′	−1.5	−1.4	−1.5	Hcat0A
5′ CA 3′ 3′ G 5′	−1.7	−0.82	−1.7	Scat15-6A, Scat15-7A, Scat15-9A, Scat15-10A
5′ TG 3′ 3′ AG 5′	−1.2	−1.12	−1.2	Hcat6A, Scat15-6A
5′ TA 3′ 3′ AA 5′	−1.0	−0.99	−1.0	Scat15-7A, S15-9A, S15-10A
5′ CU 3′ 3′ G 5′	−1.2	−0.5	−1.2	S19

[a] In the sequences of dangling-end and terminal mismatches, the T should be replaced by a U in the RNA duplex, while in the DNA duplex, the U should be replaced by a T.

dangling ends contributed to the stability of RNA/DNA hybrids in the same way they affected their respective duplexes.

The free energy of an RNA secondary structure was estimated using the *mfold* version 3.0 algorithm (*32*). The free energies of DNA secondary structures were estimated using the *mfold* algorithm with DNA parameters (*33*). The DNA hairpin H0A contains adjacent G·A mismatches and a G·G mismatch in the stem (Table 2). DNA nearest neighbor stacking energies involving these mismatches were estimated from the literature. For the dCGAC/dGGAG duplex segment in H0A, the total free energy for the three stacking interactions encompassing the two G·A mismatches at 37 °C was estimated to be −3.2 kcal/mol based on the work of Li and Agrawal (*38*). (Sequences on both sides of a / (slash) are listed in the 5′ to 3′ direction.) The influence of the G·G mismatch in the sequence dCGT/dAGG was estimated using data obtained by Peyret et al. (*39*). A value of −0.24 kcal/mol was employed for the two stacking interactions containing the G·G mismatch. The nearest neighbor stacking energies involving the C·T mismatch in the DNA hairpin H5A was obtained from Allawi and SantaLucia (*40*).

Free energy values of several single mismatches within RNA/DNA duplexes were estimated based on data from Sugimoto et al. (*41*). When data were not available for a mismatch and context of interest, data on similar sequences were employed. For example, the rC·dC mismatch in the context rCCC/dGCG occurred for the hybrid formed between several hairpin DNAs (H1A, H2A, and H3A) and the 79 nt RNA. Since data on this mismatch was unavailable, it was assigned a value of 1.3 kcal/mol based on another pyrimidine·pyrimidine mismatch, rC·dT, in the context rCCG/dGTC (*41*). Similarly, the free energy for the rA·dA mismatch in the context rUAG/dAAC was estimated to be 1.5 kcal/mol based on the average free energy for the rA·dA mismatch in rCAG/dGAC and rGAG/dCAC.

RNase H Assay. RNA and DNA were mixed in a 1x RNase H buffer containing 20 mM KCl, 10 mM $MgCl_2$, 0.1 mM EDTA, 0.1 mM DTT, 20 mM Tris-HCl, pH 7.5, and 0.1 units of prime RNase inhibitor. The solution was preincubated for 15 min at 37 °C to allow for the formation of the RNA/DNA hybrid. RNase H was then added to the mixture and incubated at 37 °C for an additional 30 min. Heating the sample at 90 °C for 3 min and quickly cooling in ice water stopped the reactions. Aliquots were then mixed with ficoll loading buffer and run on a 12% native PAGE for the 79 nt RNA or a 12% 8 M urea PAGE for the 53 nt RNA. The running buffer was 89 mM Tris-borate and 2 mM EDTA (pH 8.3). Gels were stained with ethidium bromide, and the relative intensity of the RNA bands was determined using the public domain NIH Image Analysis program for a Macintosh computer (available at http://rsb.info.nih.gov/nih-image/). Percentage degradation values were based on three repeated experiments and were reproducible within ±5%.

RESULTS

Characteristics of the Two RNA Transcripts and the DNA Oligomers. Two RNA transcripts were utilized to provide two different 15 nt long target sequences and contexts for the RNase H digestion assay. The sequence and predicted lowest energy secondary structure of the 79 nt RNA is shown in Figure 1A. The 15 nt target segment of this molecule is

Table 2: Sequence and Characteristics of the Oligodeoxynucleotides (ODNs) Targeting to the 79 nt RNA Used in the Study[a]

ODNs	Sequence	Tm	ODNs	Sequence
H0A	5'-*CCCGACGTTA***TT** |||**|*||| **C** 3'-**GGGAGGGAATCA**	60°C	S15-0A	5'-**TTCACTAAGGGAGGG**-3'
H0B	5'-*CCCTCCCTTA***TT** ||||||||||| **C** 3'-**GGGAGGGAATCA**	71.5°C	S19	5′-**GGGAG**AAATTCCATTTTC-3′
H1A	5'-*CCCTCgCTTA***TT** ||||||||||| **C** 3'-**GGGAG**c**GAATCA**	75.5°C	S15-1A	5'-**TTCACTAAG**c**GAGGG**-3'
H2A	5'-*CCCTCgCTTt***TT** ||||||||||| **C** 3'-**GGGAG**c**GAA**a**CA**	76°C	S15-2A	5'-**TTCAC**a**AAG**c**GAGGG**-3'
H2B	5'-*GGCTCCCTTA***TT** ||||||||||| **C** 3'-cc**GAGGGAATCA**	74°C	S15-2B	5'-**TTCACTAAGGGAG**cc-3'
H3A	5'-*CGCTCGCTTT***TT** ||||||||||| **C** 3'-**G**c**GAG**c**GAA**a**CA**	77°C	S15-3A	5'-**TTCAC**a**AAG**c**GAG**c**G**-3'
H4A	5'-*CCCTCCGTTA*aaa ||||||||||| a 3'-**GGGAGGGAAT**a**A**	69°C	S15-4A	5'-aaa**A**a**TAAGGGAGGG**-3'
H4B	5'-*GGCTGGCTTA***TT** ||||||||||| **C** 3'-cc**GA**cc**GAATCA**	76°C	S15-4B	5'-**TTCACTAAG**cc**AG**cc-3'
H5A	5'-*CGCACGCATA***TT** ||||||*||| **C** 3'-**G**c**G**t**G**ctt**ATCA**	59°C	S15-5A	5'-**TTCACTA**ttc**G**t**G**c**G**-3'
79 nt-RNA:	5'- GGCGAAUUGGGCCC**GUUGUCAAUAC**<u>**CCCUCCCUUAGUGAA**</u>**AUUA**GAA UUCGGUACCCCGGGUUCGAAAUCGAUAAGCU –3'			

[a] The targeted sequence in the RNA is underlined, and the target complementary bases in the ODNs are in bold. The HIV sequence in the RNA is in bold. Base changes in the target complementary region in an ODN are shown as lowercase letters. The segments in the hairpin ODNs that are not complementary to the target are shown as italicized letters. T_m values were measured in 1X RNase H buffer, pH 7.5.

shown in bold. Part of it is single stranded, while the remainder forms a duplex in the predicted structure. The next three lowest energy secondary structures also indicate the target segment to be partially single stranded and partially duplex. Previous work has shown that this 79 nt RNA can exist as a monomer or dimer depending on the sample's temperature history and environment (*25*). The monomer form of the molecule was employed in the experiments described next.

The predicted secondary structure of the 53 nt RNA transcript is shown in Figure 1B. The 15 nt target segment of this molecule contains the translation initiation site of the CAT gene and is single stranded in this lowest energy structure. This was the only structure predicted within 35% of the free energy of this structure. Nondenaturing and denaturing gel electrophoresis indicated that this transcript forms one monomer species under the conditions of the experiment.

Nine hairpin ODNs were used to direct RNase H digestion at the 15 nt region in the 79 nt RNA. The DNAs were designated H0A, H0B, H1A, H2A, H2B, H3A, H4A, H4B, and H5A and are shown in Table 2. Each is 25 nt long, and each can form a hairpin structure with a 10 bp stem and 5 base loop. H0A and H0B have the same sequence in their 5 base loop and the 3′ side of their stem. This stretch of nucleotides, shown in bold in Table 2, is complementary to the 15 nt long target segment of the 79 nt RNA (Figure 1A). H0A and H0B differ in the 5′ side of their stems. The other eight hairpin DNAs, H1A, H2A, H2B, H3A, H4A, H4B, and H5A, differ from H0B by one, two, three, four, or five base pair transversions or base substitutions in the stem or loop portion of the target binding sequence. The single-stranded DNAs, S15-0A, S15-1A, S15-2A, S15-2B, S15-3A, S15-4A, S15-4B, S15-4C, and S15-5A are 15 nt long and contain the target binding sequences of their related hairpin DNAs (Table 2).

Five DNAs that can form hairpins and five single-stranded oligomers were used in the RNase H digestion studies of the 53 nt RNA. The DNAs, Hcat0A, Hcat6A, Hcat7A, Hcat9A, and Hcat10A, are 25 nt long with 10 bp stems and 5 base loops and are shown in Table 3. The sequence of the 3′ side of the stem and the loop of Hcat0A is fully complementary to the 15 n long target segment within the 53 nt RNA. Hairpin DNAs Hcat6A, Hcat7A, Hcat9A, and Hcat10A differ from Hcat0A by six, seven, nine, and 10 base pair transversions, respectively. Single-stranded DNAs Scat15-0A, Scat15-6A, Scat15-7A, Scat15-9A, and Scat15-10A are 15 nt long and correspond to the target binding segments of their related hairpin DNAs (Table 3).

Cooperative and reversible single-step melting transitions were observed for all hairpin DNAs. T_m values are given in Tables 2 and 3. The T_m values and transition profiles were consistent with data on similar hairpin DNA structures (*42*). The 15 nt single-stranded oligonucleotides showed small (8−10%) quasi-linear increases in absorbance over the 15−90 °C temperature range with no indication of self structures.

Thermodynamic Analysis of DNA/RNA Interactions. The equilibrium binding of the hairpin DNAs to the RNA target sites was analyzed using currently available thermodynamic parameters. Although a number of kinetic factors will influence the formation of and RNase H degradation of a DNA/RNA hybrid, this study focused on the influence of DNA hairpin stability on DNA/RNA hybrid formation and the correlation of DNA/RNA stability on RNase H degradation.

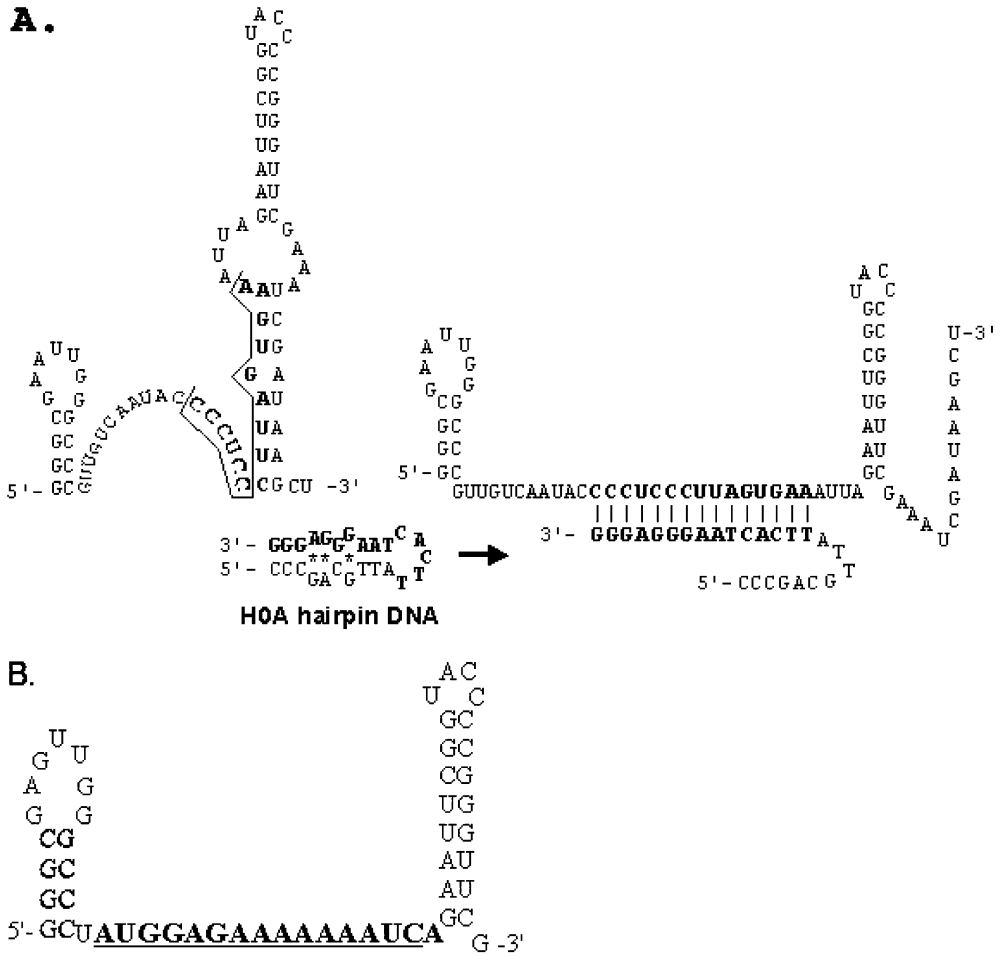

FIGURE 1: (A) Predicted secondary structure of the 79nt RNA at 37 °C using the *mfold* algorithm. The targeted RNA site is in bold and underlined. Schematic illustrates RNA−DNA formation with hairpin DNA, H0A. (B) Predicted secondary structure of the 53 nt RNA. Target site is underlined and in bold.

Table 3: Sequence and Characteristics of the Oligodeoxynucleotides (ODNs) Targeting the 53 nt RNA Used in the Study

ODNs	Sequence	Tm	ODNs	Sequence
Hcat0A	5′-*ATGGAGAAAA***GA** |||||||||| **T** 3′-**TACCTCTTTTTT**	66.7 C	Scat15-0A	5′-**GATTTTTTTCTCCAT**-3′
Hcat6A	5′-*TACCTCAAAA***GA** |||||||||| **T** 3′-atggag**TTTTTT**	66.8 C	Scat15-6A	5′-**GATTTTTTT**GAGGTA-3′
Hcat7A	5′-*TACCTCTAAA***GA** |||||||||| **T** 3′-atggaga**TTTTT**	64.9 C	Scat15-7A	5′-**GATTTTTT**AGAGGTA-3′
Hcat9A	5′-*TACCTCTTTA***GA** |||||||||| **T** 3′-atggagaaa**TTT**	64.4 C	Scat15-9A	5′-**GATTTT**AAAGAGGTA-3′
Hcat10A	5′-*TACCTCTTT***TGA** |||||||||| **T** 3′-atggagaaaa**TT**	65.8 C	Scat15-10A	5′-**GATTT**AAAAGAGGTA-3′
53 nt-RNA:	5'-GGGCGAGUUGGGCCCU**AUGGAGAAAAAAAUC**AGAAUUCGGUA CCCCGGGUUCG-3'			

The binding reaction of a hairpin DNA (D_h) with its target site on a native RNA (R_n) can be written as

$$D_h + R_n \rightleftarrows R_o{\cdot}D_s,\ \Delta G^\circ_T \quad (1)$$

The standard state free energy change, ΔG°_T, for eq 1 can be related to the free energy of forming the $R_o{\cdot}D_s$ complex from an already open RNA conformation (R_o) and the single-stranded form of the hairpin DNA (D_s)

$$R_o + D_s \rightleftarrows R_o{\cdot}D_s,\ \Delta G^\circ_1 \quad (2)$$

and the free energy corresponding to the equilibrium transition of the hairpin DNA to its single-stranded form, D_s, and the equilibrium of R_n with R_o.

$$D_s \rightleftarrows D_h,\ \Delta G^\circ_2 \quad (3a)$$

$$R_o \rightleftarrows R_n,\ \Delta G^\circ_3 \quad (3b)$$

Relating the equilibrium constants of eqs 1 to 3 yields

$$\Delta G^\circ_T = \Delta G^\circ_1 - (\Delta G^\circ_2 + \Delta G^\circ_3) \quad (4)$$

Table 4: Calculated Free Energy (ΔG) Values (kcal/mol) for the 79 nt RNA/DNA Reaction at 37 °C and the RNase H Degradation Results at 37 °C[a]

DNA	$\Delta G°_1$* [b]	$\Delta G°_1$ [c]	$\Delta G°_2$ [d]	$\Delta G°_3$ [e]	$\Delta G_{37}°_T$ [f]	% RNA degradation 37 °C (0.5 U)	% RNA degradation 37 °C (5 U)
H0A	−13.8	−14.9	−5.7	−2.7	−6.5	79	83
H0B	−13.8	−14.9	−9.8	−2.7	−2.4	52	78
S15-0A	−13.8	−14.9	0	−2.7	−12.2	91	95
H1A	−9.5	−10.6	−10.5	−2.7	2.6	0	0
S15-1A	−9.5	−10.6	0	−2.7	−7.9	83	95
H2A	−6.25	−7.35	−10.9	−2.7	6.25	0	0
S15-2A	−6.25	−7.35	0	−2.7	−4.65	2	38
H2B	−10.8	−12.3	−10.2	−2.7	0.6	38	46
S15-2B	−10.8	−12.3	0	−2.7	−9.6	89	96
H3A	−3.25	−4.75	−11.7	−2.7	9.7	0	5
S15-3A	−3.25	−4.75	0	−2.7	−2.05	0	10
H4A	−8.1	−9.2	−10.2	−2.7	3.7	30	31
S15-4A	−8.1	−9.2	0	−2.7	−6.5	35	38
H4B	−5.5	−7.0	−10.8	−2.7	6.5	7	17
S15-4B	−5.5	−7.0	0	−2.7	−4.3	67	90
H5A	−5.0	−6.6	−6.6	−2.7	2.7	0	12
S15-5A	−5.0	−6.6	−1.0	−2.7	−2.9	0	18
S19	−3.7	−6.4	0	−2.7	−3.7	5	28

[a] The RNase H assays were done at 37 °C for 30 min with 0.5 U or 5 U RNase H, 15 pmol of RNA, and 90 pmol of DNA in a total volume of 10 μL. [b] $\Delta G°_1{}^*$ is the free energy change for forming the $R_o{\cdot}D_s$ complex from an already open RNA conformation (R_o) and the single-stranded form of a DNA (D_s), which does not consider the dangling-end/terminal mismatch effects. [c] $\Delta G°_1$ is the estimated free energy change for forming the $R_o{\cdot}D_s$ complex from an already open RNA conformation (R_o) and the single-stranded form of a DNA (D_s), which includes the free energy contributions from terminal mismatches/dangling ends. [d] $\Delta G°_2$ is the free energy changes of forming the structured DNA (D_s) from the single-strand DNA (D_s). [e] $\Delta G°_3$ the free energy changes of forming the native RNA structure (R_n) from the partially unfolded RNA structure (R_o). R_o is the lowest free energy structure with the target sequence constrained to be single stranded. [f] $\Delta G_{37}°_T$ is the standard state free energy for the overall reaction between DNA and RNA.

$\Delta G°_3$ was calculated for the 79 nt RNA using the Zuker algorithm assuming R_n to be the predicted lowest free energy structure and R_o to be the lowest free energy structure with the 15 nt target sequence constrained to be single stranded. $\Delta G°_3 = 0$ for the 53 nt RNA since the target site of this molecule is single stranded in its predicted lowest energy structure. Thermodynamic parameters described in the Materials and Methods were used for the free energy calculations. Similar calculations carried out previously for the 79 nt RNA (*25*) ignored dangling ends and terminal mismatches and employed an earlier set of parameters.

The standard state free energy change ($\Delta G°_T$) for binding hairpin and single-stranded DNAs to the 79 and 53 nt RNA at 37 °C are listed in Tables 4 and 5, respectively, using the above model and assumptions. For example, the predicted free energy for the interaction of H0A with the 79 nt RNA is $\Delta G°_T = -6.5$ kcal/mol. This value is based on $\Delta G°_1 = -14.9$ kcal/mol, $\Delta G°_2 = -5.7$ kcal/mol, and $\Delta G°_3 = -2.7$ kcal/mol. Terminal mismatches/dangling-ends contributed −1.1 kcal/mol to the free energy of interaction of H0A with the 79 nt RNA, $\Delta G°_1$. The free energy contributions of the different reaction steps to the overall free energy change for binding the DNA oligomers to the two RNAs are listed in Tables 4 and 5. Previous work using the above approach with different parameters showed that the predicted amount of RNA/DNA hybrid formed between several DNAs listed in Table 4 and the 79 nt RNA were in qualitative accord with gel mobility shift binding data (*25*). This outcome is unchanged using the updated parameters of the current study.

Table 5: RNase H Degradation Results at 37 °C and the Estimated ΔG Value (kcal/mol) for Each 53 nt RNA/DNA Reaction[a]

DNA	$\Delta G°_1$*	$\Delta G°_1$	$\Delta G°_2$	$\Delta G_{37}°_T$	% RNA degradation 0.5 D/R	% RNA degradation 4.5 D/R
Hcat0A	−10.2	−12.0	−8.2	−3.8	82	100
Scat15−0A	−10.2	−12.2	0.0	−12.2	100	100
Hcat6A	−3.2	−6.1	−8.0	1.9	33	100
Scat15−6A	−3.2	−6.1	0.0	−6.1	100	100
Hcat7A	−2.8	−5.3	−7.4	2.1	20	40
Scat15−7A	−2.8	−5.5	0.0	−5.5	95	100
Hcat9A	−2.0	−4.5	−8.1	3.6	0	4
Scat15−9A	−2.0	−4.7	0.0	−4.7	35	95
Hcat10A	−2.6	−5.1	−8.5	3.4	0	0
Scat15−10A	−1.6	−4.3	0.0	−4.3	0	50

[a] The RNase H assays were done at 37 °C for 30 min with 0.25 U of RNase H in a volume of 8 or 10 μL. Data are shown for ratios of 10 pmol of DNA to 20 pmol of RNA (0.5 D/R) and for 90 pmol of DNA to 20 pmol of RNA (4.5 D/R). Free energy terms in this table are the same as in Table 4. $\Delta G°_3$ is zero for all cases, and this column is not shown.

RNase H Degradation of the 79 nt RNA. RNase H degradation of the 79 nt RNA was examined in the presence of hairpin and single-stranded DNA oligomers with sequences fully or partially complimentary to the 15 nt target site. Figure 2 shows results of incubating 0.5 units of RNase H for 30 min with 9 μM various DNAs and 1.5 μM 79 nt RNA. Using these assay conditions, the fully complimentary hairpin H0A induced approximately 80% degradation of the RNA (Table 4). The 6:1 ratio of DNA to RNA was used for all DNAs in the assay. Lane 1 of panels A−C of Figure 2 shows controls of the RNA alone with the RNase H enzyme. The single band in each case corresponds to the undigested 79 nt RNA. Lanes 2−9 in panels A and B and lanes 2−5 in panel C of Figure 2 show the results of the RNase H degradation assay directed by the DNAs listed in Table 2. Similar reactions were also performed using 5 units of RNase H using the same amounts of RNA and DNA (not shown). Table 4 lists the extent of RNA degradation in the 37 °C assay using 0.5 and 5 units of RNase H.

H0A degraded 79% of the RNA using 0.5 units of RNase H at 37 °C, while H0B produced 50% degradation under the same conditions (Table 4, Figure 2A). Both DNAs have the same fully complementary target binding sequence but the less stable hairpin, H0A, produced greater degradation. The single-stranded control for these two hairpins, S15-0A, has the same 15 nt complementary sequence and produced 91% degradation. When the assay was performed with 5 units of RNase H, the percentage of degradation was similar for H0A (83%) and H0B (78%), and degradation directed by S15-0A was essentially complete (Table 4).

The hairpin DNA H1A has a one base pair change relative to H0B creating 5 and 9 nt long target complementary segments separated by a mismatched base. Although the single-stranded DNA control for this hairpin, S15-1A, directed 83% degradation, H1A produced no degradation. The predicted free energy of forming the H1A/RNA hybrid was +2.6 kcal/mol as compared to the free energies of −6.5

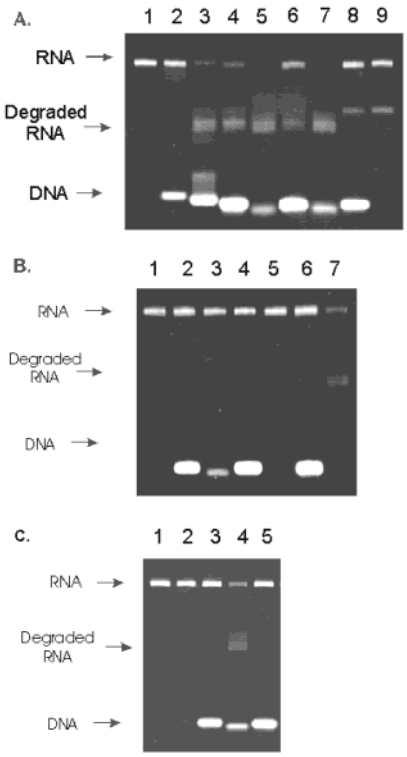

FIGURE 2: RNase H degradation assay of 79 nt RNA. A total of 15 pmol of RNA were incubated with 90 pmol of DNA and 0.5 unit of RNase H for 30 min. Reaction products were run on a 12% native PAG. Lane 1 in panels A−C contained RNA alone with the RNase H enzyme. (A) Lanes 2−9: RNA with RNase H and S19, H0A, H0B, S15-0A, H2B, S15-2B, H4A, and S15-4A, respectively. (B) Lanes 2−7: 79 nt RNA with RNase H and H5A, S15-5A, H3A, S15-3A, H4B, and S15-4B, respectively. (C) Lanes 2−5: 79 nt RNA with S15-2A, H2A, S15-1A, and H1A, respectively.

and −2.4 kcal/mol for H0A and H0B, respectively (Table 4). Hairpins H2A and H2B have two base pair changes as compared to H0B. The base changes in H2A result in segments 5, 3, and 5 nt long that are complementary to the RNA target, while the changes in H2B result in a 13 nt complementary segment. The predicted $\Delta G°_T$ of the H2B/RNA hybrid was 0.6 kcal/mol, and it directed 38% RNA degradation (Figure 2A, Table 3). The $\Delta G°_T$ of forming a H2A/RNA hybrid was +6.25 kcal/mol, and neither H2A nor its single-stranded control S15-2A produced measurable degradation of the 79 nt RNA (Figure 2C). The inability of S15-2A to direct RNase H degradation may be due to the short lengths of its complementary segments. The $\Delta G°_T$ of the S15-2A/RNA hybrid, −4.65 kcal/mol, is similar to the hybrid formed by S15-4B that directed significantly more degradation. However, the latter ODN has a 9 nt long complementary segment. S19, a single-stranded ODN with a 5 nt segment complementary to the RNA, produced no more than 5% degradation. Previous studies have shown that a minimum size of four RNA/DNA base pairs is required for *E. coli* RNase H degradation (*43*). When excess RNase H was employed in the assay (5 units), increased degradation was observed for both S15-2A and S19 (Table 3).

H3A and H5A and their single-stranded controls S15-3A and S15-5A did not direct degradation under the 0.5 U RNase H assay conditions (Figure 2B, Table 4). The effect of changing the hairpin loop sequence of H0B on RNase H cleavage was examined using H4A. Four of the five nucleotides in the loop were changed leaving a 10 nt target

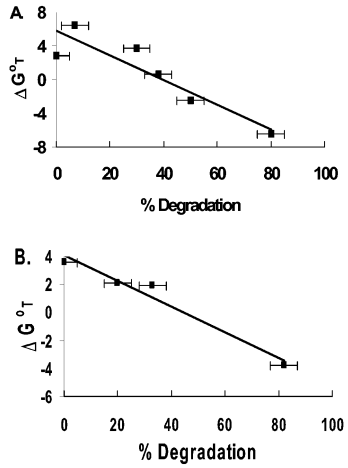

FIGURE 3: (A) Percent degradation of 79 nt RNA in assay with 0.5 U RNase H and 6:1 DNA/RNA vs free energy of formation for an RNA/DNA duplex for hairpin DNAs H0A, H0B, H1A, H2B, H4A, and H4B. (B) Percent degradation of 53 nt RNA in assay with 0.25 U RNase H and 0.5:1 DNA/RNA vs free energy of formation of DNA/RNA for hairpin DNAs Hcat0A, Hcat6A, Hcat7A, and Hcat9A.

complimentary segment. H4A caused 30% degradation (lane 8, Figure 2A). This indicates that complementary base pairing in the loop is not essential for degradation. Surprisingly, the corresponding single-stranded DNA, S15-4A, caused a similar amount of degradation (35%). A possible explanation for the relatively low percentage of degradation directed by S15-4A is an intramolecular self-structure due to the AGGG repeat (*44*). Although this cannot be ruled out, absorbance versus temperature analysis did not show characteristics of a cooperative transition. H4B with four base changes distributed in the target binding region did not direct significant RNase H degradation (≤7%), while S15-4B, its single-stranded control, produced 67% degradation.

Figure 3A plots the percentage of RNA degraded versus the $\Delta G°_T$ of formation of DNA/RNA hybrids for hairpin DNAs in Table 4. Data on H2A, H3A, and H5A were excluded from the plot since their single-stranded controls did not direct RNase H degradation. The linear regression has a correlation coefficient of $R^2 = 0.84$. While the extent of degradation in this assay is expected to depend on a number of factors (e.g., the length of the complementary segments, rate of RNA/DNA formation), Figure 3A indicates that to the first approximation, hairpin DNA induced degradation is linearly correlated to the free energy required to form the RNA/DNA hybrid. Data on all 15 nt single-stranded ODNs in Table 4 give a similar linear regression with a correlation coefficient of 0.73 (not shown).

RNase H Degradation of the 53 nt RNA. Figure 1B shows the second RNA target site examined, a 15 nt purine rich translation initiation sequence of the CAT gene imbedded in a 53 nt RNA. Since the target site is predicted to be single stranded, it is expected to be more accessible than the 79 nt RNA target site. In addition, the DNA/RNA hybrid of the second target site will be predominantly rR/dY. This hybrid is generally more stable than the homologous DNA duplex, d*R*/d*Y*, in the hairpin DNA (*45*).

RNase H assays showed that the 53 nt RNA required less enzyme and less DNA then the 79 nt RNA to achieve comparable levels of degradation. Figure 4 displays results

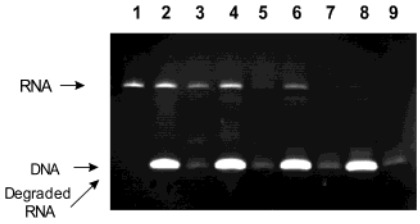

FIGURE 4: RNase H degradation assay of 53 nt RNA. A total of 0.25 units of RNase H were incubated with 20 pmol of RNA and 90 pmol of DNA for 30 min. Reaction products were run on a 12% 8 M urea PAG. Lanes 1−9: 53 nt RNA only, 53 nt RNA with Hcat10A, Scat15-10A, Hcat9A, Scat15-9A, Hcat7A, Scat15-7A, Hcat6A, and Scat15-6A, respectively.

for a 30 min RNase H assay at 37 °C conducted with the 53 nt RNA and hairpin DNAs Hcat6A, Hcat7A, Hcat9A, and Hcat10A and single-stranded DNAs Scat15-6A, Scat15-7A, Scat15-9A, and Scat15-10A. Table 5 lists the extent of degradation of the 53 nt RNA for the DNAs employed using the conditions described in Figure 4. Although the DNA to RNA ratio was 4.5:1 and only 0.25 units of RNase H were employed, Hcat6A with only a 9 nt complementary segment caused complete RNA degradation (Figure 4, lane 8). By comparison, H4B, which also has a 9 nt segment complementary to its target site in the 79 nt RNA, caused only 7% degradation with twice as much RNase H and a 6:1 ratio of DNA to RNA (Table 4). Hcat9A and Hcat10A did not cause RNA degradation, but Scat15-9A and Scat15-10A with 6 and 5 nt long complementary segments caused 96 and 49% degradation, respectively (Figure 4, Table 5). The single strands S19 and S15-5A have 5 and 7 nt long segments directed at the 79 nt RNA target site but produced 5% or less degradation with twice as much RNase H and a 6:1 ratio of DNA to RNA (Table 4).

To compare the effect of DNA/RNA stability on RNase H degradation of the 53 nt RNA with results from the 79 nt RNA, conditions were sought that produced ~80% degradation with the fully complementary Hcat0A. The 80% degradation level was observed for the 79 nt RNA with its fully complementary hairpin H0A. A DNA/RNA ratio of 0.5:1 with 0.25 U RNase H was found to achieve 80% degradation of the 53 nt RNA in the 30 min assay. Table 5 lists the results using these conditions. The single-stranded ODNs Scat15-6A and Scat15-7A degrade the RNA completely (95−100%), while their hairpin DNA counterparts, Hcat 6A and Hcat7A, produced 33 and 20% degradation. This illustrates the impact of the hairpin secondary structure on reducing the free energy for DNA/RNA hybrid formation and on RNase H degradation. Figure 3B plots the correlation between the percent degradation of the 53 nt RNA and the $\Delta G°_T$ of hybrid formation for the Hcat DNA hairpins. The linear regression has a correlation coefficient of 0.96. This result, like the result in Figure 3A, supports the notion that under appropriate conditions, RNA degradation directed by stable hairpin DNAs is correlated to the free energy needed to open the DNA hairpin stem and form a RNA/DNA hybrid.

DISCUSSION

The traditional view of a successful antisense ODN is one that exhibits strong binding to its cellular RNA target. Most antisense ODNs are designed to maximize their binding to the RNA target and are generally single stranded. A side effect may arise if the ODN binds and affects closely related RNA sequences. In instances where RNase H plays a major role in an application of an antisense ODN, the enzyme may degrade RNA/DNA hybrids with partial complementarity. The minimum size of an RNA/DNA hybrid cleaved by an RNase H is reported to be 4 bp for the calf thymus RNase H at 32 °C (*46*), 4 bp for the *E. coli* RNase H at 37 °C (*43*), and 6 bp for human RNase H1 at 37 °C (*47*). Our results show that the *E. coli* RNase HI can efficiently digest RNA with single-stranded DNAs that have only five bases complementary to a target sequence (Scat15-10A). RNase H-competent single-stranded antisense ODNs have the potential to cause cleavage at many nontargeted cellular RNA sequences. Poor sequence specificity has been observed with PS-DNAs in cell-free translation systems (*48, 49*).

The results from this study show that the effectiveness and stringency of RNase H degradation can be influenced by the stability of the RNA/DNA hybrid and competing DNA secondary structure. All of the single-stranded DNAs that produced substantive degradation generated less degradation when they were part of a hairpin structure. Under appropriate conditions, both the 79 and 53 nt RNA showed a linear correlation between the extent of degradation directed by a hairpin DNA and the free energy needed to form the RNA/DNA hybrid (Figure 3). A one base pair change in the hairpin DNA H0A (H0B to H1A) resulted in a large attenuation of RNase H degradation of the 79 nt RNA. The same base pair change in the single-stranded S15 0A did not produce a corresponding level of response. Modulating the stability of a hairpin DNA and/or the RNA/DNA hybrid can affect the stringency of RNase H degradation.

The results also point out that a stringency effect is minimized when RNA/DNA formation is sufficiently favorable to overcome the influence of a competing DNA secondary structure. This was observed for the 53 nt RNA at the 4.5:1 ratio of DNA to RNA. The hairpin DNA Hcat6A was as effective as Hcat0A in the RNase H assay.

As noted in our previous work (*25*), degradation produced by DNA hairpins with unfavorable free energies for RNA/DNA formation can only be understood if RNase H promotes hybrid formation. Under the reaction conditions employed, the equilibrium reaction of the RNA and DNA alone predicts a negligible amount of hybrid formation. A detailed analysis of DNA directed cleavage of an RNA target site must include kinetic analysis of DNA/RNA substrate formation, the influence of RNase H on hybrid formation, and the rate of RNase H cleavage. In this study, we focused only on the correlation between the free energy of formation of the RNA/DNA complex and the extent of RNase H degradation. The results indicate that the stability of the RNA/DNA complex is an important component of the reaction and that competing DNA secondary structures can enhance the specificity of DNA directed RNase H cleavage.

REFERENCES

1. Monia, B. P., Lesnik, E. A., Gonzalez, C., Lima, W. F., McGee, D., Guinosso, C. J., Kawasaki, A. M., Cook, P. D., and Freier, S. M. (1993) Evaluation of 2′-modified oligonucleotides containing 2′-deoxy gaps as antisense inhibitors of gene expression, *J. Biol. Chem. 268*, 14514−22.
2. Boiziau, C., Tarrago-Litvak, L., Sinha, N. D., Moreau, S., Litvak, S., and Toulme, J. J. (1996) Antisense oligonucleotides inhibit in vitro cDNA synthesis by HIV-1 reverse transcriptase, *Antisense Nucleic Acid Drug Dev. 6*, 103−9.

3. ten Asbroek, A. L., van Groenigen, M., Nooij, M., and Baas, F. (2002) The involvement of human ribonucleases H1 and H2 in the variation of response of cells to antisense phosphorothioate oligonucleotides, *Eur. J. Biochem. 269*, 583−92.
4. Dean, N. M. (2001) Functional genomics and target validation approaches using antisense oligonucleotide technology, *Curr. Opin. Biotechnol. 12*, 622−5.
5. Khare, M. D., and Sharland, M. (2001) Cytomegalovirus treatment options in immunocompromised patients, *Expert Opin. Pharmacother. 2*, 1247−57.
6. Witherell, G. W. (2001) ISIS-14803, *Curr. Opin. Investig. Drugs 2*, 1523−1529.
7. Chi, K. N., Gleave, M. E., Klasa, R., Murray, N., Bryce, C., Lopes de Menezes, D. E., D'Aloisio, S., and Tolcher, A. W. (2001) A phase I dose-finding study of combined treatment with an antisense Bcl-2 oligonucleotide and mitoxantrone in patients with metastatic hormone-refractory prostate cancer, *Clin. Cancer Res. 7*, 3920−7.
8. Flaherty, K. T., Stevenson, J. P., and O'Dwyer, P. J. (2001) Antisense therapeutics: lessons from early clinical trials, *Curr. Opin. Oncol. 13*, 499−505.
9. Morse, M. A. (2001) Technology evaluation: ISIS-2503, *Curr. Opin. Mol. Ther. 3*, 589−94.
10. Morris, M. J., Tong, W. P., Cordon-Cardo, C., Drobnjak, M., Kelly, W. K., Slovin, S. F., Terry, K. L., Siedlecki, K., Swanson, P., Rafi, M., DiPaola, R. S., Rosen, N., and Scher, H. I. (2002) Phase I trial of BCL-2 antisense oligonucleotide (G3139) administered by continuous intravenous infusion in patients with advanced cancer, *Clin. Cancer Res. 8*, 679−83.
11. Kausch, I., Lingnau, A., Endl, E., Sellmann, K., Deinert, I., Ratliff, T. L., Jocham, D., Sczakiel, G., Gerdes, J., and Bohle, A. (2003) Antisense treatment against Ki-67 mRNA inhibits proliferation and tumor growth in vitro and in vivo, *Int. J. Cancer 105*, 710−6.
12. Luger, S. M., O'Brien, S. G., Ratajczak, J., Ratajczak, M. Z., Mick, R., Stadtmauer, E. A., Nowell, P. C., Goldman, J. M., and Gewirtz, A. M. (2002) Oligodeoxynucleotide mediated inhibition of *c*-myb gene expression in autografted bone marrow, *Blood 99*, 1150−8.
13. Hibi, T., Inoue, N., Ogata, H., and Naganuma, M. (2003) Introduction and overview: recent advances in the immunotherapy of inflammatory bowel disease, *J. Gastroenterol. 38*, 36−42.
14. Gilar, M., Belenky, A., Smisek, D. L., Bourque, A., and Cohen, A. S. (1997) Kinetics of phosphorothioate oligonucleotide metabolism in biological fluids, *Nucleic Acid Res. 25*, 3615−20.
15. Hudziak, R. M., Barofsky, E., Barofsky, D. F., Weller, D. L., Huang, S. B., and Weller, D. D. (1996) Resistance of morpholino phosphorodiamidate oligomers to enzymatic degradation, *Antisense Nucleic Acid Drug Dev. 6*, 267−72.
16. Summerton, J. (1999) Morpholino antisense oligomers: the case for an RNase H-independent structural type, *Biochim. Biophys. Acta 1489*, 141−58.
17. Crinelli, R., Bianchi, M., Gentilini, L., and Magnani, M. (2002) Design and characterization of decoy oligonucleotides containing locked nucleic acids, *Nucleic Acids Res. 30*, 2435−43.
18. Woolf, T. M., Melton, D. A., and Jennings, C. G. (1992) Specificity of antisense oligonucleotides in vivo, *Proc. Natl. Acad. Sci. U.S.A. 89*, 7305−9.
19. Zhou, W., and Agrawal, S. (1998) Mixed-backbone oligonucleotides as second-generation antisense agents with reduced phosphorothioate-related side effects, *Bioorg. Med. Chem. Lett. 8*, 3269−74.
20. Shen, L. X., Kandimalla, E. R., and Agrawal, S. (1998) Impact of mixed-backbone oligonucleotides on target binding affinity and target cleaving specificity and selectivity by *Escherichia coli* RNase H, *Bioorg. Med. Chem. 6*, 1695−705.
21. Agrawal, S. (1999) Importance of nucleotide sequence and chemical modifications of antisense oligonucleotides, *Biochim. Biophys. Acta 1489*, 53−68.
22. Wang, H., Cai, Q., Zeng, X., Yu, D., Agrawal, S., and Zhang, R. (1999) Antitumor activity and pharmacokinetics of a mixed-backbone antisense oligonucleotide targeted to the RIα subunit of protein kinase A after oral administration, *Proc. Natl. Acad. Sci. U.S.A. 96*, 13989−94.
23. Wang, H., Wang, S., Nan, L., Yu, D., Agrawal, S., and Zhang, R. (2002) Antisense anti-MDM2 mixed-backbone oligonucleotides enhance therapeutic efficacy of topoisomerase I inhibitor irinotecan in nude mice bearing human cancer xenografts: in vivo activity and mechanisms, *Int. J. Oncol. 20*, 745−752.
24. Lok, C. N., Viazovkina, E., Min, K. L., Nagy, E., Wilds, C. J., Damha, M. J., and Parniak, M. A. (2002) Potent gene-specific inhibitory properties of mixed-backbone antisense oligonucleotides comprised of 2′-deoxy-2′-fluoro-D-arabinose and 2′-deoxyribose nucleotides, *Biochemistry 41*, 3457−67.
25. Li, J., and Wartell, R. M. (1998) RNase H1 can catalyze RNA/DNA hybrid formation and cleavage with stable hairpin or duplex DNA oligomers, *Biochemistry 37*, 5154−61.
26. Agrawal, S., Temsamani, J., and Tang, J.-Y. (1991) Pharmacokinetics, biodistribution, and stability of oligodeoxynucleotide phosphorothioates in mice, *Proc. Natl. Acad. Sci. U.S.A. 88*, 7595−9.
27. Rebowski, G., Wojcik, M., Boczkowska, M., Gendaszewska, E., Soszynski, M., Bartosz, G., and Niewiarowski, W. (2001) Antisense hairpin loop oligonucleotides as inhibitors of expression of multidrug resistance-associated protein 1: their stability in fetal calf serum and human plasma, *Acta Biochim. Pol. 48*, 1061−76.
28. Lautenberger, J. A. (1991) A computer program to assist in the preparation of oligonucleotide solutions, *BioTechniques 10*, 778−80.
29. Sambrook, J., Fritsch, E. F., and Maniatis, T. (1989) *Molecular Cloning: Laboratory Manual*, 2nd ed., p E.5, Cold Spring Harbor Laboratory Press, Woodbury, New York.
30. Serra, M. J., and Turner, D. H. (1995) Predicting thermodynamic properties of RNA, *Methods Enzymol. 259*, 242−61.
31. SantaLucia, J., Jr., and Turner, D. H. (1997) Measuring the thermodynamics of RNA secondary structure formation, *Biopolymers 44*, 309−19.
32. Mathews, D. H., Sabina, J., Zuker, M., and Turner, D. H. (1999) Expanded sequence dependence of thermodynamic parameters improves prediction of RNA secondary structure, *J. Mol. Biol. 288*, 911−40.
33. SantaLucia, J., Jr. (1998) A unified view of polymer, dumbbell, and oligonucleotide DNA nearest-neighbor thermodynamics, *Proc. Natl. Acad. Sci. U.S.A. 95*, 1460−5.
34. Sugimoto, N., Nakano, S., Katoh, M., Matsumura, A., Nakamuta, H., Ohmichi, T., Yoneyama, M., and Sasaki, M. (1995) Thermodynamic parameters to predict stability of RNA/DNA hybrid duplexes, *Biochemistry 34*, 11211−6.
35. Wu, P., Nakano, S.-I., and Sugimoto, N. (2002) Temperature dependence of thermodynamic properties for DNA/DNA and RNA/DNA duplex formation, *Eur. J. Biochem. 269*, 2821−30.
36. Bommarito, S., Peyret, N., and SantaLucia, J., Jr. (2000) Thermodynamic parameters for DNA sequences with dangling ends, *Nucleic Acids Res. 28*, 1929−34.
37. Ohmichi, T., Nakano, S., Miyoshi, D., and Sugimoto, N. (2002) Long RNA dangling end has large energetic contribution to duplex stability, *J. Am. Chem. Soc. 124*, 10367−72.
38. Li, Y., and Agrawal, S. (1995) Oligonucleotides containing G. A pairs: effect of flanking sequences on structure and stability, *Biochemistry 34*, 10056−62.
39. Peyret, N., Seneviratne, P. A., Allawi, H. T., and SantaLucia, J., Jr (1999) Nearest-neighbor thermodynamics and NMR of DNA sequences with internal A·A, C·C, G·G, and T·T mismatches, *Biochemistry 38*, 3468−77.
40. Allawi, H. T., and SantaLucia, J., Jr. (1998) Thermodynamics of internal C·T mismatches in DNA, *Nucleic Acids Res. 26*, 2694−701.
41. Sugimoto, N., Nakano, M., and Nakano, S. (2000) Thermodynamics−structure relationship of single mismatches in RNA/DNA duplexes, *Biochemistry 19*, 11270−81.
42. Paner, T. M., Amaratunga, M., Doktycz, M. J., and Benight, A. S. (1990) Analysis of melting transitions of the DNA hairpins formed from the oligomer sequences d[GGATAC(X)4GTATCC], *Biopolymers 29*, 1715−34.
43. Hogrefe, H. H., Hogrefe, R. I., Walder, R. Y., and Walder, J. A. (1990) Kinetic analysis of *Escherichia coli* RNase H using DNA-RNA-DNA/DNA substrates, *J. Biol. Chem. 265*, 5561−6.
44. Huertas, D., and Azorin, F. (1996) Structural polymorphism of homopurine DNA sequences. d(GGA)n and d(GGGA)n repeats form intramolecular hairpins stabilized by different base-pairing interactions, *Biochemistry 35*, 13125−35.
45. Lesnik, E. A., and Freier, S. M. (1995) Relative thermodynamic stability of DNA, RNA, and DNA:RNA hybrid duplexes: relationship with base composition and structure, *Biochemistry 34*, 10807−15.
46. Donis-Keller, H. (1979) Site-specific enzymatic cleavage of RNA, *Nucleic Acids Res. 7*, 179−92.

47. Wu, H., Lima, W. F., and Crooke, S. T. (1999) Properties of cloned and expressed human RNase H1, *J. Biol. Chem. 274*, 28270−8.
48. Stein, D., Foster, E., Huang, S. B., Weller, D., and Summerton, J. (1997) A specificity comparison of four antisense types: morpholino, 2′-*O*-methyl RNA, DNA, and phosphorothioate DNA, *Antisense Nucleic Acid Drug Dev. 7*, 151−7.
49. Larrouy, B., Boiziau, C., Sproat, B., and Toulme, J. J. (1995) RNase H is responsible for the nonspecific inhibition of in vitro translation by 2′-*O*-alkyl chimeric oligonucleotides: high affinity or selectivity, a dilemma to design antisense oligomers, *Nucleic Acids Res. 23*, 3434−40.

BI034897Z